North Atlantic Ocean Wave Climate Change Scenarios for the Twenty-First Century

XIAOLAN L. WANG, FRANCIS W. ZWIERS, AND VAL R. SWAIL

Climate Research Branch, Meteorological Service of Canada, Downsview, Ontario, Canada

(Manuscript received 28 March 2003, in final form 16 December 2003)

ABSTRACT

Using the observed relationships between sea level pressure (SLP) and significant wave height (SWH) as represented by regression models, climate change scenarios of SWH in the North Atlantic were constructed by means of redundancy analysis (for seasonal means and 90th percentiles of SWH) and nonstationary generalized extreme value analysis (for seasonal extreme SWH). SWH scenarios are constructed using output from a coupled climate model under three different forcing scenarios. Scenarios of future anomaly seasonal statistics of SWH are constructed using climate model projections of anomaly seasonal mean SLP while projections of seasonal extreme SWH are made using projections of seasonal mean SLP and seasonal SLP gradient index. The projected changes in SWH are assessed by means of a trend analysis.

The northeast Atlantic is projected to have increases in both winter and fall seasonal means and extremes of SWH in the twenty-first century under all three forcing scenarios. These changes are generally accompanied by decreases in the midlatitudes of the North Atlantic and increases in the southwest North Atlantic. The rate and sign of the projected SWH change is not constant throughout the twenty-first century. In the Norwegian and North Seas, the projected SWH changes are characterized either by faster increases in the late decades than in the early decades, or by decreases in the early decades followed by increases, depending on the forcing scenario and the specific location. Using lower or higher rates of increase in greenhouse gases forcing generally leads to reduced or increased rates of change, respectively, in ocean wave heights. The sign and rate of future wave height changes in the North Sea in particular appear to be quite dependent on the forcing conditions. In general, global warming is associated with more frequent occurrence of the positive phase of the North Atlantic Oscillation (NAO) and strong cyclones, which leads to increases of wave heights in the northeast Atlantic.

1. Introduction

The earth's climate is constantly changing. In addition to natural variabilities, future climate will also be influenced by anthropogenic emissions of greenhouse gases (GHG) and aerosols. The tools currently available for simulating the response of the climate system to the changing atmospheric composition are global climate models. Descriptions of the modeled response of the climate system to scenarios of anthropogenic forcing are referred to as climate projections. With the exception of some restricted oceanic regions in some models, all regions of the globe are projected to show warming under the enhanced GHG conditions that are anticipated to prevail in the late decades of the twenty-first century. Global mean temperature is projected to rise by 1.4 to 5.8 K between 1990 and 2100 (Houghton et al. 2001) for the full range of Special Report on Emissions Scenarios (SRES; Nakicenovic and Swart 2000) forcing scenarios. The corresponding rise in sea level is projected to be 0.09 to 0.88 m (Houghton et al. 2001).

Corresponding author address: Dr. Xiaolan L. Wang, Climate Research Branch, Meteorological Service of Canada, 4905 Dufferin Street, Downsview, ON M3H 5T4, Canada.
E-mail: Xiaolan.Wang@ec.gc.ca

The oceans are an important component of the climate system and oceanborne commerce is sensitive to the state of the ocean surface. Among other surface characteristics, ocean wave height could be affected by anthropogenic forcing of the climate system. Since the design of offshore oil platforms and other marine and coastal infrastructure is constrained by the largest wave height event anticipated during a fixed design period, increases in the extremes of wave height could have an impact on the life span of these installations that will be in excess of impacts anticipated from the rising sea level.

Projections of ocean wave height are therefore useful for the design and operation of coastal and offshore industries. However, previous studies in this field are limited. The STOWASUS-2100 (Regional Storm, Wave, and Surge Scenarios for the 2100 Century) Group (Kaas and the STOWASUS Group 2001) carried out two 30-yr time-slice experiments for the northeast Atlantic: a control run for the period of 1970–99, and a double CO_2 run for the period of 2060–89. The WASA (Waves and Storms in the North Atlantic) Group (1998) carried out a similar pair of 5-yr time-slice experiments for the North Atlantic as well as producing a statistical projection of future anomalies of intramonthly quantiles of

wave height at Brent and near Ekofisk (in the northern and central North Sea, respectively). Given the intensity of industrial activity in parts of the North Atlantic, and the intensity of ship traffic throughout the basin, there is a need for additional projections of the future wave height climate that span the entire basin. The purpose of this study is to construct climate change scenarios of wave height in the North Atlantic, and to carry out a detailed assessment of changes in the projected wave heights.

Strictly speaking, a climate change scenario refers to the difference between some plausible future climate and the current or control climate (usually as represented in a climate model). Such differences can be viewed as an interim step towards constructing a climate scenario—a plausible future climate that has been constructed for explicit use in investigating the potential consequences of anthropogenic climate change (Houghton et al. 2001). Climate scenarios should represent future conditions that account for both human-induced climate change and natural climate variability. Such scenarios often make use of climate projections, by manipulating model outputs and combining them with observed climate data.

Although global climate models (GCMs) are fundamental for constructing climate scenarios, the direct use of GCM output for impact assessment is limited by a number of factors. For example, most climate change scenarios derived from GCMs are presented at coarse spatial resolutions; and some types of climate variables needed for quantitative impacts studies, such as ocean wave heights or storm surge frequencies, are not directly available from GCMs. Building on the assumption that the regional climate is conditioned by the large-scale atmospheric state, both dynamical models (e.g., regional climate models, or RCMs) and empirical/statistical methods have been developed for ''downscaling'' GCM-projected climate changes (i.e., to construct climate change scenarios on regional scales, or to provide information about other climate variables that are not simulated by contemporary climate models). Both approaches have their relative strengths and weaknesses (Houghton et al. 2001).

We use an empirical approach based on linear regression in this study. Our approach is the classical one that has been used in empirical downscaling work. We use a regression model to represent the relationship between large-scale atmospheric conditions and ocean wave heights on the seasonal time scale in the observed climate of the past several decades. We then assume that this relationship will continue to hold under the possible future climates as projected by a coupled global climate model. The model we use is CGCM2, the second-generation coupled GCM of the Canadian Centre for Climate Modelling and Analysis (Flato and Boer 2001). Our decision to use the empirical approach is based on our previous experience with the analysis of the wave climate of the latter half of the twentieth century and the reconstruction of the wave climate of the early part of the twentieth century (Wang and Swail 2001, 2002). The empirical relationships that we exploit rely, primarily, on the large-scale structure of the North Atlantic sea level pressure (SLP) field as represented by its low-order empirical orthogonal functions (EOFs). The EOFs, which are derived from observations, represent the climate model simulated SLP variability well, both in the twentieth and twenty-first centuries. Thus the nature of the large-scale circulation variability in the future climate as simulated by CGCM2 is similar to that of the present day. Hence, links between that variability and the variability of SWH should also continue to hold in the future.

The remainder of this paper is organized as follows: The datasets and methodologies used in this study are briefly described in sections 2 and 3, respectively. The wave height climate change scenarios and the implications of climate change for extreme wave height events are presented in section 4. Finally, a summary and discussion is presented in section 5 to conclude this paper.

2. Datasets

There is a strong relationship between storm track variations and the large-scale, low-frequency variability in the mean flow (Lau 1988; Chang and Fu 2003). Consistent with this are the findings of our previous studies (Wang and Swail 2002, 2001), which showed that seasonal significant wave height (SWH) variations in the North Atlantic over the 1958–97 period are closely associated with contemporaneous seasonal mean SLP variations in the region, especially in winter [January–February–March (JFM)] and fall [October–November–December (OND)]. This suggests that SLP can be used to predict SWH, and that it may be possible to project changes in the SWH climate by using GCM projected changes in the SLP climate. This approach was adopted in this study. Since the SLP–SWH relationship is much more profound in the cold seasons (winter and fall) than in the warm seasons [April–May–June (AMJ) and July–August–September (JAS)], we will focus only on the cold seasons in the present study. The observed SLP–SWH relationship in each season will be represented by a pair of regression models, one for seasonal means and 90th–percentiles of SWH, and a second for seasonal maxima of SWH.

Observations of seasonal mean SLP, and of seasonal means, 90th-percentiles, and maxima of SWH are needed to train our statistical models. The wave height data used in this study are derived from a 40-yr hindcast of ocean waves in the North Atlantic for the period from 1958–97 (Swail and Cox 2000), which has been produced for assessment of the observed climate and variability of the oceanic waves. The hindcast (i.e., prediction for a past period) was obtained by driving a third-generation ocean wave model (OWI 3G; see the

appendix in Wang and Swail 2002 for more details) with surface winds over the North Atlantic basin that were intensively reanalyzed (Wang and Swail 2002; Swail and Cox 2000). The resulting ocean wave height dataset has complete spatial and temporal coverage for the 40-yr reanalysis period, and compares well with both altimeter and in situ data (Swail and Cox 2000; Cox et al. 2001). The hindcasts are available at 6-hourly intervals on a 0.625° latitude by 0.833° longitude grid over the North Atlantic (20°–70°N, 80°W–20°E). Seasonal means, 90th-percentiles, and maxima of SWH were derived from the 6-hourly wave data and reexpressed as anomalies relative to the baseline climate of 1961–90. These anomalies were used as the predictand data when training our statistical models.

Similarly, seasonal means of SLP for 1958–97 were derived from the twice-daily National Centers for Environmental Prediction–National Center for Atmospheric Research (NCEP–NCAR) reanalysis (Kalnay et al. 1996) and expressed as anomalies relative to the climate of 1961–90. These data had previously be converted to the global 96 × 48 Gaussian grid (approximately 3.75° latitude × 3.75° longitude) used by CGCM2. Only those data over the Atlantic sector (16.7°–72.36°N, 82.5°W–22.5°E) were used in this study. The squared gradients of monthly mean SLP were also calculated from monthly means of SLP, and subsequently seasonally averaged. The monthly and seasonal squared gradient indices were then expressed as anomalies relative to their 1961–90 baseline climates, which in turn, were used as predictors when training our regression models.

Projections of future SLP anomalies were obtained from three ensembles of CGCM2 simulations (monthly mean SLP) using three different forcing scenarios: (i) a modified version of the Intergovernmental Panel on Climate Change (IPCC) IS92a scenario, in which the change in GHG forcing corresponds to that observed from 1850 to 1990 and increases at a rate of 1% yr^{-1} thereafter until year 2100 (cf. Boer et al. 2000); (ii) the SRES A2 forcing scenario, which is described in detail in the Special Report on Emissions Scenarios (Nakicenovic and Swart 2000); and (iii) the SRES B2 forcing scenario. The forcing includes both greenhouse gas and aerosol loadings. The A2 scenario is similar to the IS92a scenario. The B2 scenario reflects slower economic development and population growth and thus a slower increase in GHG forcing.

An ensemble of three integrations was available for each forcing scenario, with each individual integration being initiated from different initial conditions. The integration period is 251 yr (1850–2100) for the IS92a scenario and 111 yr (1990–2100) for both the A2 and B2 scenarios. The initial conditions for the A2 and B2 integrations were taken from the IS92a integration. The differences between the individual integrations in an ensemble are entirely due to natural variability (Flato and Boer 2001). Thus, the three members of each ensemble can be considered as three independent realizations of the same stochastic process.

The CGCM2 simulated baseline (1961–90) climate was calculated from the IS92a scenario ensemble simulations and subtracted from the CGCM2 simulated seasonal means of SLP to obtain anomalies of seasonal mean SLP simulated for each of the three forcing scenarios. CGCM2 simulated SLP squared gradient indices were obtained from the simulated monthly means of SLP that were adjusted to the observed baseline climate (by replacing the simulated baseline climate with the observed baseline climate as derived from the NCEP reanalysis). The CGCM2 simulated anomalies of seasonal mean SLP and squared SLP gradient indices were then used as predictors in the SLP–SWH regression relationship to project possible future anomalies of the seasonal means and extremes of SWH (see sections 3a,b).

3. Methodologies

a. Redundancy analysis

The observed relationship between seasonal means of SLP and seasonal means (or 90th percentiles) of SWH was determined by using a least squares regression technique called redundancy analysis (RA). Redundancy analysis is similar to canonical correlation analysis (CCA) in the sense that both methods seek to derive a hierarchy of correlated pairs of the predictor and the predictand components. However, RA and CCA use different criteria to identify predictor and predictand relationships. While CCA aims to maximize the correlation between components, RA seeks to maximize the proportion of predictand variance that is predicted for each component. Thus, RA's asymmetrical treatment of predictor and predictand is better suited for situations where the objective is to specify the behavior of one variable on the basis of that of another.

Specifically, RA is used to identify patterns of different fields ($\mathbf{X}$ and $\mathbf{Y}$) that are linked through the regression model:

$$\hat{\mathbf{Y}} = \mu_{\mathbf{Y}} + \mathbf{C}_{\mathbf{YX}}\mathbf{C}_{\mathbf{XX}}^{-1}(\mathbf{X} - \mu_{\mathbf{X}}), \tag{1}$$

where $\hat{\mathbf{Y}}$ is a linear prediction of $\mathbf{Y}$, $\mu_{\mathbf{X}}$ and $\mu_{\mathbf{Y}}$ are the expected values of $\mathbf{X}$ and $\mathbf{Y}$, respectively, and $\mathbf{C}_{\mathbf{XX}}$ and $\mathbf{C}_{\mathbf{YX}}$ are the covariance and cross-covariance matrices. Redundancy analysis maximizes the predicted variance, finds a hierarchy of orthogonal predictand modes, and associates them with the corresponding predictor patterns. The jth predictand mode identified by RA is the jth EOF of the prediction $\hat{\mathbf{Y}}$. The temporal variations of the jth best correlated pair of the predictor and the predictand modes are referred to as the jth RA components (RAC_j). The proportion of the total variance in $\mathbf{Y}$ which is predicted by the linear prediction $\hat{\mathbf{Y}}$ is called the redundancy index, denoted as R^2. More details about RA can be found in Wang and Swail (2001, 2002), Wang

TABLE 1. Redundancy index (R^2) of the RA model for seasonal SWH statistics (means and 90th percentiles; also denoted as Havg and Hp90, respectively) over the North Atlantic, as well as the correlation coefficients between the observed and RA-predicted leading PCs, and between the observed and RA-predicted leading RA components (RACs) of SWH statistics for winter (JFM) and fall (OND). Also shown are the percentages of the total variance in the SWH statistics (P_{SWH}) or in the seasonal mean fields of SLP or seasonal SLP gradient index (P_{SLP}) that are associated with the 7 retained EOFs for each season (12 retained EOFs when the seasonal SLP gradient index is used as predictor).

Predictor		P_{SLP}		P_{SWH}	R^2	PC1	PC2	PC3	RAC1	RAC2	RAC3
Seasonal mean SLP	JFM	94.0	Havg	89.3	0.96	0.96	0.79	0.55	0.95	0.84	0.71
			Hp90	85.1	0.87	0.93	0.78	0.48	0.93	0.80	0.67
	OND	90.9	Havg	83.3	0.81	0.79	0.90	0.75	0.81	0.90	0.80
			Hp90	78.7	0.72	0.78	0.77	0.69	0.81	0.79	0.70
Seasonal SLP gradient index	JFM	91.9	Havg	94.5	0.87	0.91	0.60	0.37	0.91	0.72	0.30
			Hp90	91.7	0.80	0.85	0.66	0.54	0.87	0.69	0.45
	OND	86.7	Havg	90.8	0.82	0.77	0.75	0.32	0.79	0.77	0.61
			Hp90	87.9	0.78	0.67	0.58	0.40	0.78	0.64	0.66

and Zwiers (2001), von Storch and Zwiers (1999), and Tyler (1982).

We also tried to use the seasonal SLP squared gradient index as predictor in the RA analysis and found that it was not quite as good a predictor for SWH as seasonal mean SLP. This is probably because the seasonal squared gradient index is not a better indicator of storm track activity as seasonal mean SLP. Low pressure features in the seasonal mean SLP field are well correlated with high magnitude SWH features because these mean SLP features arise in a given area only when it is traversed by large numbers of synoptic systems. Therefore, we decided to use seasonal mean SLP as the predictor of the corresponding seasonal SWH statistics (means or 90th-percentiles).

The RA analysis was performed in reduced dimension versions of the predictor and predictand datasets so as to focus attention on their large-scale behavior. Bearing in mind the related eigenspectra, we compared the ''predictive'' skills of RA models with between 4 and 13 leading SLP and SWH principal components (PCs). We found that the best skill is obtained when the seven leading PCs of SWH and SLP are retained. Twelve PCs are required when the seasonal SLP gradient index is used as the predictor. Thus, the retained leading PCs of the SWH and SLP anomalies were used instead of the original datasets in the RA-regression analysis. The percentage of the total variance associated with the retained PCs/EOFs (also called the retained variance) is listed in Table 1. This percentage ranges from 80% to 90% for seasonal mean SWH, and 91%–94% for the observed seasonal mean SLP (NCEP reanalysis). Most importantly, the observed changes in SWH and SLP are well represented in the retained leading PCs/EOFs. For example, changes of winter SWH in the North Atlantic are well represented by the first principal component of SWH (Wang and Swail 2002).

There is evidence in the literature suggesting that one of the climate's responses to external forcing may be a change in the occupation statistics of its preferred modes of variability, rather than changes in the modes themselves (Palmer 1999; Monahan et al. 2000). Thus we projected the CGCM2 simulated SLP anomalies onto the retained EOFs derived from NCEP reanalysis to obtain seven simulated pseudo-PCs of SLP anomalies. These seven pseudo-PCs explain 87%–89% (82%–85%) of the total simulated variance of winter (fall) SLP anomalies and well represent the trends and large-scale variabilities of the projected SLP.

The regression model used in the RA analysis was trained using detrended anomalies of seasonal means (or 90th-percentiles) of SWH, derived from 6-hourly hindcast wave data, and detrended anomalies of seasonal mean SLP or the seasonal SLP gradient index from the NCEP reanalysis for the 40-yr period from 1958 to 1997. Both predictor and predictand were of reduced dimension as explained earlier. The training was performed with linearly detrended anomalies to ensure that the fitted model was not influenced by artificial dependencies resulting from, for example, the response of the observed SLP field to anthropogenic forcing (e.g., Gillett et al. 2003).

Table 1 shows three measures of the predictive skill of the RA regression: 1) the proportion (R^2) of the predictand variance that can be predicted by the RA regression, 2) the correlation coefficients between the three leading pairs of observed and RA-predicted PCs, and 3) the correlation coefficients between the three leading pairs of observed and predicted RA components (RACs) of seasonal means and 90th-percentiles of SWH. The regression using seasonal mean SLP as the predictor can explain about 96% (87%) of the total retained variance of seasonal means (90th-percentiles) of SWH in winter, and about 81% (72%) in fall. Thus the link between SLP and SWH is somewhat stronger in winter than in autumn, and it is stronger for mean SWH than for seasonal extremes of SWH. In particular, the first two PCs, which well represent trends and large-scale variabilities of SWH, were very well ''predicted'' in the RA regression. The link between the seasonal SLP gradient index and SWH are similar in strength to those between seasonal mean SLP and SWH, although

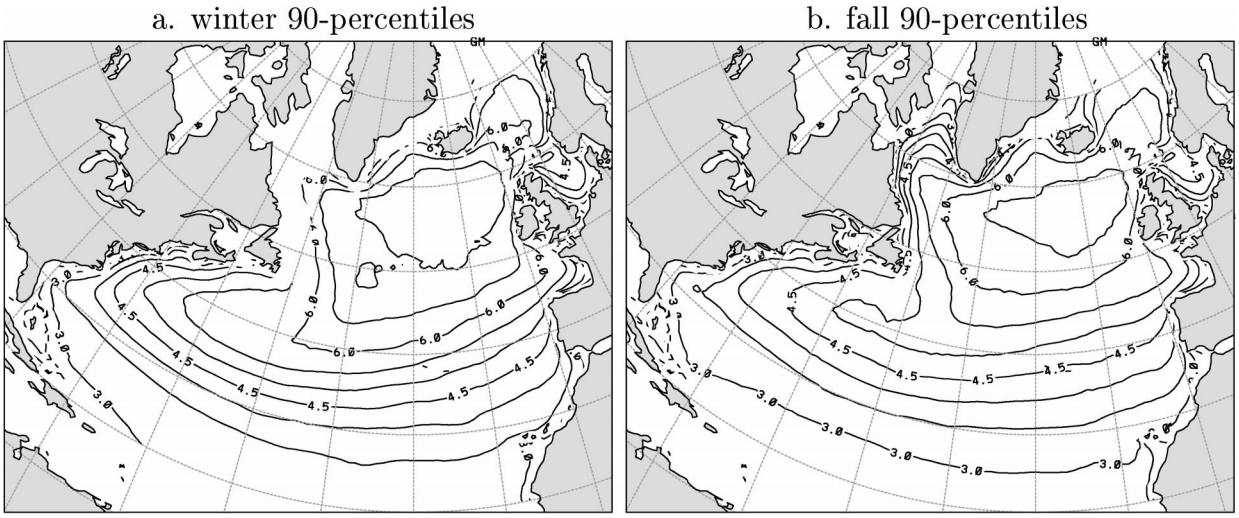

FIG. 1. The baseline (1961–90) climate values of winter and fall seasonal 90th percentiles of SWH in the North Atlantic. The contour interval is 0.5 m.

this gradient index is not quite as good a predictor for SWH as the seasonal mean SLP (it has slightly lower correlation coefficients between the observed and predicted PCs or RACs; cf. the PCs and RACs columns in Table 1).

CGCM2 simulated anomalies of seasonal mean SLP (also of reduced dimension, but not detrended) were then substituted into the RA regression model to project future anomalies of seasonal SWH statistics (means and 90th-percentiles) of reduced dimension. These EOF-space projections were then converted back to physical space. Each projected anomaly field of SWH statistics obtained in this way was then superimposed on the corresponding field of observed baseline climate of SWH statistics (shown in Fig. 1 for the 90th percentiles) to obtain a projection of the full field for that statistic. A separate projection was produced using the SLP anomalies derived from each member of each three-member ensemble of CGCM2 simulations, resulting in an ensemble of three projections of seasonal SWH statistics (means or 90th-percentiles) for each of the three forcing scenarios. These projections of SWH were then analyzed to assess future trends in ocean wave heights (see sections 3c and 4a).

b. Nonstationary generalized extreme value (GEV) analysis

Since non-Gaussian behavior is a particular concern for extremes, statistical models for data of Gaussian distribution (such as redundancy analysis or other conventional regression models) are not really suitable for analyzing extremes. Further, if the earth's climate is changing, then its extremes are most likely those of a nonstationary process, which will have characteristics that change systematically through time. In this case, the classical stationary generalized extreme value (GEV) model (with constant parameters) is no longer appropriate (Leadbetter et al. 1983). One should allow the GEV parameters to change through time in order to represent the systematically changing characteristics of extremes. A GEV model of time-varying parameters is called a nonstationary GEV model (Coles 2001).

In this study, we carried out the nonstationary GEV analysis to characterize the SWH extremes of the changing climate, to make projections of future extreme wave heights. We first fit nonstationary GEV models to the observed seasonal maxima of SWH, in which one or more of the GEV parameters are assumed to be a function of atmospheric variables that are thought to affect SWH extremes. Then, the CGCM2 projections of the atmospheric variables for 1990–2099 are used to vary the parameters of the GEV model to produce projections of future extremes (see section 4).

Specifically, the GEV family has distribution functions of the form

$$G(z) = \exp\left\{-\left[1 + \xi\left(\frac{z-\mu}{\sigma}\right)\right]^{-1/\xi}\right\};$$
$$-\infty < \mu < \infty, \quad \sigma > 0, \quad -\infty < \xi < \infty,$$

where μ, σ, and ξ are the location, scale, and shape parameters, respectively (Coles 2001). These parameters could change as a result of climate change. However, the shape parameter of a GEV distribution is difficult to estimate with precision, so it is usually unrealistic to try modeling ξ as a smooth function of time or one or more time-dependent covariate(s). In this study, we assume that ξ will not change as a result of climate change. We do, however, allow the location and scale parameters to vary with time-dependent covariates.

Let the notation GEV (μ, σ, ξ) denote the GEV distribution with location parameter μ, scale parameter σ, and shape parameter ξ. Then, the following five nested GEV models were fitted to the observed seasonal maxima of SWH (derived from the 40-yr wave hindcast) at each grid point.

- GEV_0 (μ, σ, ξ). In this model all parameters are constant.
- GEV_1 ($\mu_t = \mu_o + r_1 P_t$, σ, ξ). In this model the location parameter is a function of the time-dependent covariate P_t.
- GEV_2 ($\mu_t = \mu_o + r_1 P_t + r_2 G_t$, σ, ξ). In this model the location parameter is a function of two time-dependent covariates, P_t and G_t.
- GEV_3 ($\mu_t = \mu_o + r_1 P_t + r_2 G_t$, $\log(\sigma_t) = b_o + q_1 P_t$, ξ). In this model the location parameter is a function of two covariates (P_t and G_t), and the scale parameter is a function of one covariate (P_t).
- GEV_4 ($\mu_t = \mu_o + r_1 P_t + r_2 G_t$, $\log(\sigma_t) = b_o + q_1 P_t + q_2 G_t$, ξ). In this model the location and scale parameters are both functions of P_t and G_t.

The time-dependent covariates used in these models, P_t and G_t, are, respectively, the seasonal mean SLP anomaly and the seasonal squared SLP gradient index at the SWH grid point. Note that these SLP quantities, which are required on the fine SWH grid, were calculated from values at four nearest SLP grid points (all within about 500-km radius from the SWH grid point), using weights proportional to the inverse of the distance. Here, P_t contains information about the mean state of SLP at time t, and G_t contains information about its variation in space, over the area within 500-km radius from the SWH grid point.

The previously described GEV models were trained using observed P_t and G_t as derived from the NCEP reanalysis for the 1958–97 period. The significance of the linear relationships built into the various GEV models (and the goodness of fit of the GEV models themselves) was assessed by performing the following likelihood ratio tests. Let L_i denote the maximum log-likelihood for model GEV_i ($i = 0, 1, 2, 3, 4$). Then, a test of the validity of model GEV_j relative to model GEV_i ($i < j$) at the p level of significance (here $p = 0.05$) is to reject model GEV_i in favor of model GEV_j if the deviance statistic

$$D_{ji} = 2(L_j - L_i) > \chi_k^2(p),$$

where $\chi_k^2(p)$ is the $(1 - p)$ quantile of the χ^2 distribution with k degrees of freedom, where k is the difference between the number of estimated parameters in models GEV_j and GEV_i.

Likelihood ratio tests were carried out to assess model GEV_i ($i = 1, 2, 3, 4$) relative to model GEV_{i-1} (and to model GEV_0 for $i = 2, 3, 4$). Results of these tests, which are summarized in Table 2, show that the location parameter for the SWH extremes is significantly correlated with both the anomalies of seasonal mean SLP (P_t) and the seasonal SLP gradient index (G_t; see r_1 and r_2 in Table 2 and Fig. 2). However, the results also show that the scale parameter appears to be independent of either P_t or G_t (and hence does not change with time; see q_1 and q_2 in Table 2).

TABLE 2. The field significance (Livezey and Chen 1983) of the regression parameters r_1, r_2, q_1, and q_2 (see section 3b), as represented by the percentages of grid points where a given GEV model is favored over a relatively simpler GEV model at the 5% level of significance.

	JFM	OND
GEV_1 over GEV_0 (r_1)	54.0	44.8
GEV_2 over GEV_1 (r_2)	43.6	29.7
GEV_2 over GEV_0 (r_1 and r_2)	70.3	53.1
GEV_3 over GEV_2 (q_1)	2.3	2.2
GEV_3 over GEV_0 (r_1, r_2, and q_1)	31.2	21.4
GEV_4 over GEV_3 (q_2)	1.4	1.0
GEV_4 over GEV_0 (r_1, r_2, q_1, and q_2)	10.4	8.4

Based on this analysis, we chose to use the fitted GEV_2 model to project possible future changes in SWH extremes. To this end, the CGCM2 simulated values of P_t and G_t were substituted into the fitted expression for the location parameter,

$$\hat{\mu}_t = \hat{\mu}_o + \hat{r}_1 P_t + \hat{r}_2 G_t,$$

to produce a time series of location parameter estimates for the 1990–2099 period. This time series was then analyzed as outlined in section 3c to estimate trends in the location parameter of SWH extremes. These trends, in turn, were used to project changes in the size and frequency of extreme SWH events.

c. *Analysis of projected trends*

In this section we report on our analysis of trends in the projected SWH statistics. We study trends in the projected seasonal means and 90th percentiles of SWH, and in the projected location parameter $\hat{\mu}_t$ of the distribution of the seasonal extremes of SWH.

Let x_t denote the projected time series that is to be analyzed. The following regression models (RMs) were fitted to x_t at each grid point:

- RM_0: $x_t = \alpha_0 + \varepsilon_t$ (i.e., no trend in x_t);
- RM_1: $x_t = \alpha_0 + \alpha_1 t + \varepsilon_t$ (i.e., linear trend in x_t);
- RM_2: $x_t = \alpha_0 + \alpha_1 t + \alpha_2 t^2 + \varepsilon_t$ (i.e., quadratic trend in x_t),

where α_i are the regression parameters, and ε_t denotes a zero-mean white noise process. Standard F tests (e.g., Venables and Ripley 1999) were used to intercompare pairs of models RM_j and RM_i ($j > i$).

The sample that we used to perform the trend analysis for each forcing scenario was obtained by combining the three members of each ensemble into a single sample with three ''observations'' at each sampling time. Thus, the series length is $n = (3 \times 110)$. Results of the F tests are summarized in Table 3 and will be discussed in detail in sections 4a and 4b.

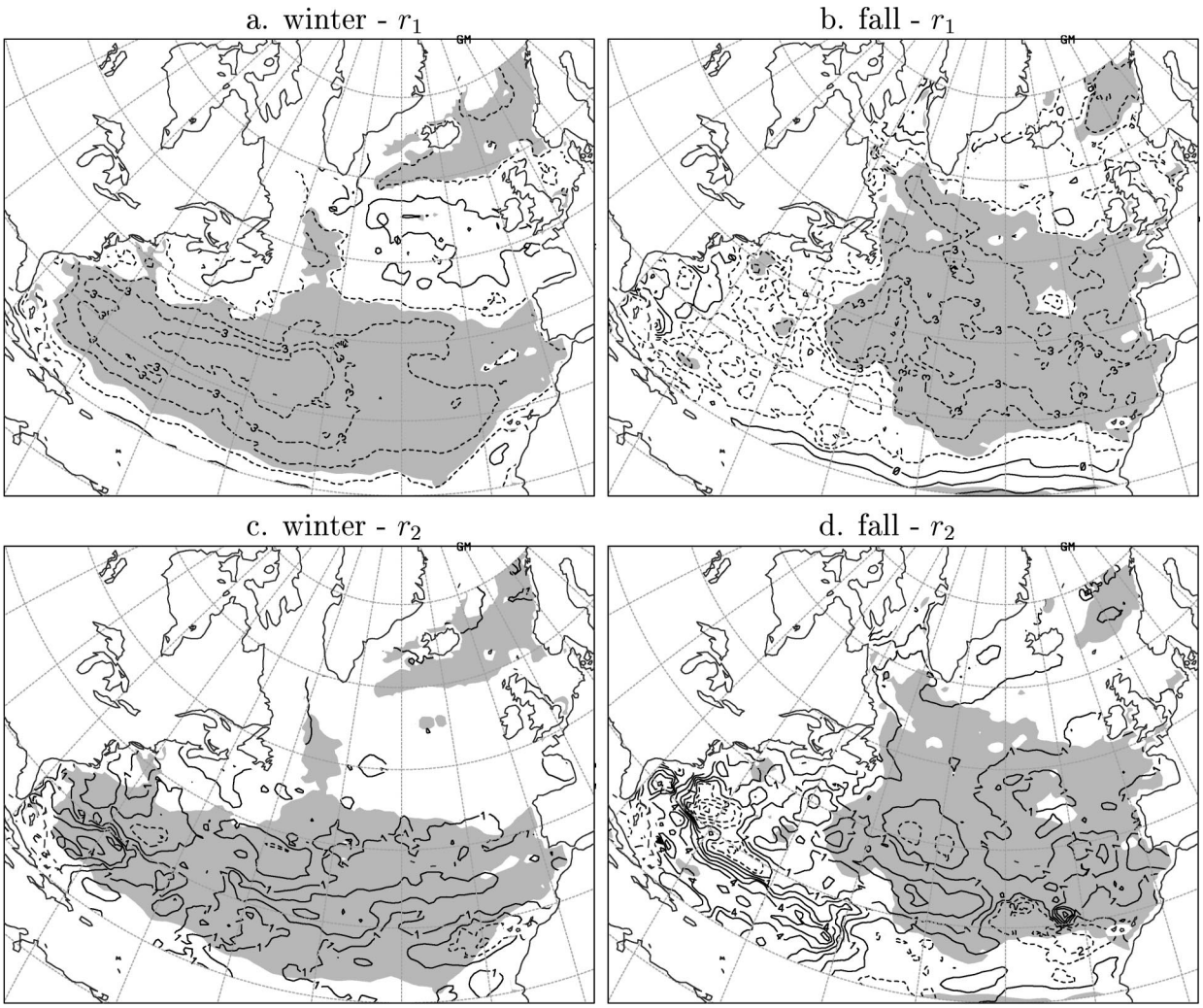

FIG. 2. The estimated coefficients linking the GEV location parameter for seasonal maximum SWH with anomalies of seasonal mean SLP (r_1 from GEV_1) or seasonal SLP gradient index (r_2 from GEV_2). The contour interval is 1.0. Shading indicates locations where the coefficient is significantly (at 5% level) different from zero (results of χ^2 tests that compare GEV_1 with GEV_0 for significance of r_1, and GEV_2 with GEV_1 for significance of r_2. See section 3b and Table 2 for the percentages of the shaded areas).

TABLE 3. The field significance of trends in the seasonal statistics (means and 90th percentiles), and in the GEV location parameter $\hat{\mu}_t$ of seasonal maxima, of SWH projected with the three forcing scenarios, as represented by the percentages of grid points where a RM model is favored over a relatively simpler RM model at the 5% level of significance (see section 3c). Bold entries represent cases where a linear representation of trend is not sufficient.

		Means		90th percentiles		$\hat{\mu}_t$	
Scenario	Models tested	JFM	OND	JFM	OND	JFM	OND
IS92a	RM_1 over RM_0	67.7	26.8	61.3	74.7	59.2	54.2
	RM_2 over RM_0	69.5	20.0	61.3	67.4	59.3	48.8
	RM_2 over RM_1	**23.5**	0.0	**22.2**	0.0	**10.2**	6.3
A2	RM_1 over RM_0	61.1	60.0	54.7	70.0	61.7	55.0
	RM_2 over RM_0	75.7	54.5	67.9	63.6	60.3	51.2
	RM_2 over RM_1	**47.7**	4.2	**39.4**	4.0	**14.6**	6.7
B2	RM_1 over RM_0	45.3	6.9	34.7	33.9	51.5	32.5
	RM_2 over RM_0	44.3	1.0	36.3	29.8	53.6	22.7
	RM_2 over RM_1	**9.1**	0.0	**11.2**	0.5	**9.7**	0.9

In addition, the Durbin–Watson statistic was also calculated to test the null hypothesis that the residual time series of the previously selected regression model is white. Evidence counter to the null hypothesis was not found.

4. Ocean wave height climate change scenarios

In this section, we describe changes in seasonal statistics (means and 90th percentiles) of SWH projected with the three different forcing scenarios for the 1990–2099 period, as well as the implications for extreme wave height events. The changes of a SWH statistic are expressed in physical units and as percentages of its baseline climate value. Figure 1 shows the typical climate field of SWH in the North Atlantic, featuring a center of high waves in the region west of Ireland (50°–60°N): In the cold seasons, the typical values of seasonal means, 90th percentiles, and maxima of SWH in this region are 4–5, 6–8, and 11–13 m, respectively. Corresponding values in the Norwegian Sea are 3–4, 5–6, and 9–11 m, respectively, and 2–3, 3–5, and 6–9 m in the North Sea.

a. Trends/changes in the projected seasonal statistics of SWH

Using datasets described in section 2 and the RA regression technique described in section 3a, for each of the three forcing scenarios, we constructed an ensemble of three projections for each of the seasonal statistics (means and 90th percentiles) of SWH for winter (JFM) and fall (OND) of the 1990–2099 period. Trends in the projected 1990–2099 time series of seasonal SWH statistics at each grid point were analyzed as described in section 3c. Results are summarized in Table 3. As expected, trends are more apparent under the strong IS92a and A2 forcing than under the weaker B2 forcing. Also, for the seasonal mean SWH, trends are more apparent in the winter solstice season than in the preceding transition season (i.e., fall).

In the strong forcing cases, a simple linear representation of trend is not sufficient in many locations, especially in winter (cf. the bold numbers in Table 3). For example, in the Norwegian and North Seas, trends are more or less quadratic, with either faster increases in the late decades than in the first few decades, or decreases in the first few decades followed by increases in the later decades of the twenty-first century (cf. Figs. 3a–f, which show typical trends of SWH in the northeast Atlantic). In the following we discuss changes in SWH that are projected with RM_2 because the quadratic components of trends are not negligible, especially in winter (also note that the estimate $\hat{\alpha}_2$ will be near zero if the trend is basically linear).

The locations with statistically significant (at 5% level) quadratic trends in the projected seasonal mean SWH are shaded in Fig. 4. This diagram also shows the change in the seasonal mean SWH in the 90-yr period from 1990 to 2080 as estimated using RM_2 (i.e., $\hat{h}_{tr}(t) = \hat{\alpha}_o + \hat{\alpha}_1 t + \hat{\alpha}_2 t^2$). Changes in winter seasonal mean SWH projected under IS92a forcing for 2020 and 2050 are displayed in Fig. 5. Figure 4 shows that while the three scenarios have generally similar patterns of change in both winter and fall, the changes projected under the IS92a and A2 scenarios are generally larger and more extensive than those under the B2 scenario. Overall, similar forcing scenarios (IS92a and A2) lead to similar changes in seasonal mean SWH, and a scenario (B2) with a slower rate of increase in GHG forcing leads to smaller changes in seasonal mean SWH. However, note that stronger changes are projected in the northeast Atlantic (including the North Sea) for the A2 scenario, and in the southwest North Atlantic for the IS92a scenario (cf. Figs. 4a and 4c).

In winter, as shown at left in Fig. 4, the patterns of change in seasonal mean SWH are commonly characterized by increases of up to 12 cm (or 5% of the baseline climate values) in the southwest North Atlantic, matched by decreases of up to 20 cm in the midlatitudes. For the northeast Atlantic, especially for the North Sea, the projected future seasonal mean SWH changes were found to be quite dependent on the forcing conditions. Quadratic trends with decreases in the first few decades of the 1990–2099 period followed by increases were projected with the IS92a scenario (cf. Figs. 3a, 4a, and 5), while large and basically linear increases (up to 32 cm or 11% of the baseline climate values) were projected with the A2 scenario (cf. Figs. 3b and 4c), and no significant changes were projected with the B2 scenario (cf. Fig. 4e).

The pattern of the projected changes in the fall mean SWH (cf. Fig. 4, right) are similar to those of winter, but the changes are generally smaller and less extensive (see also Table 3). In this season, quadratic components of trends were found to be less extensive in general; and they are more apparent for the A2 scenario rather than for the IS92a scenario (it is the other way around in winter; see Figs. 3a,b and 3d,e).

The projected pattern of changes for the 90th percentiles of winter SWH, and the differences between scenarios (not shown), are similar to those projected for the seasonal means, except that the area of increase in the northeast Atlantic extends farther to the northwest for the 90th-percentiles than for the seasonal means projected with the A2 scenario (cf. Figs. 4c and 6a). From 1990 to 2080, the increase in the northeast Atlantic is as large as 55 cm for the 90th percentiles (which is also about 11% of the relevant baseline climate value).

The projected patterns of change in the 90th percentiles of fall SWH are a little different from those of the corresponding seasonal mean in the lower latitudes: Increases of up to 50 cm (9% of the baseline climate values) were projected for the 90th percentiles in the central subtropical North Atlantic (cf. Fig. 6b), but no significant changes were projected for the seasonal

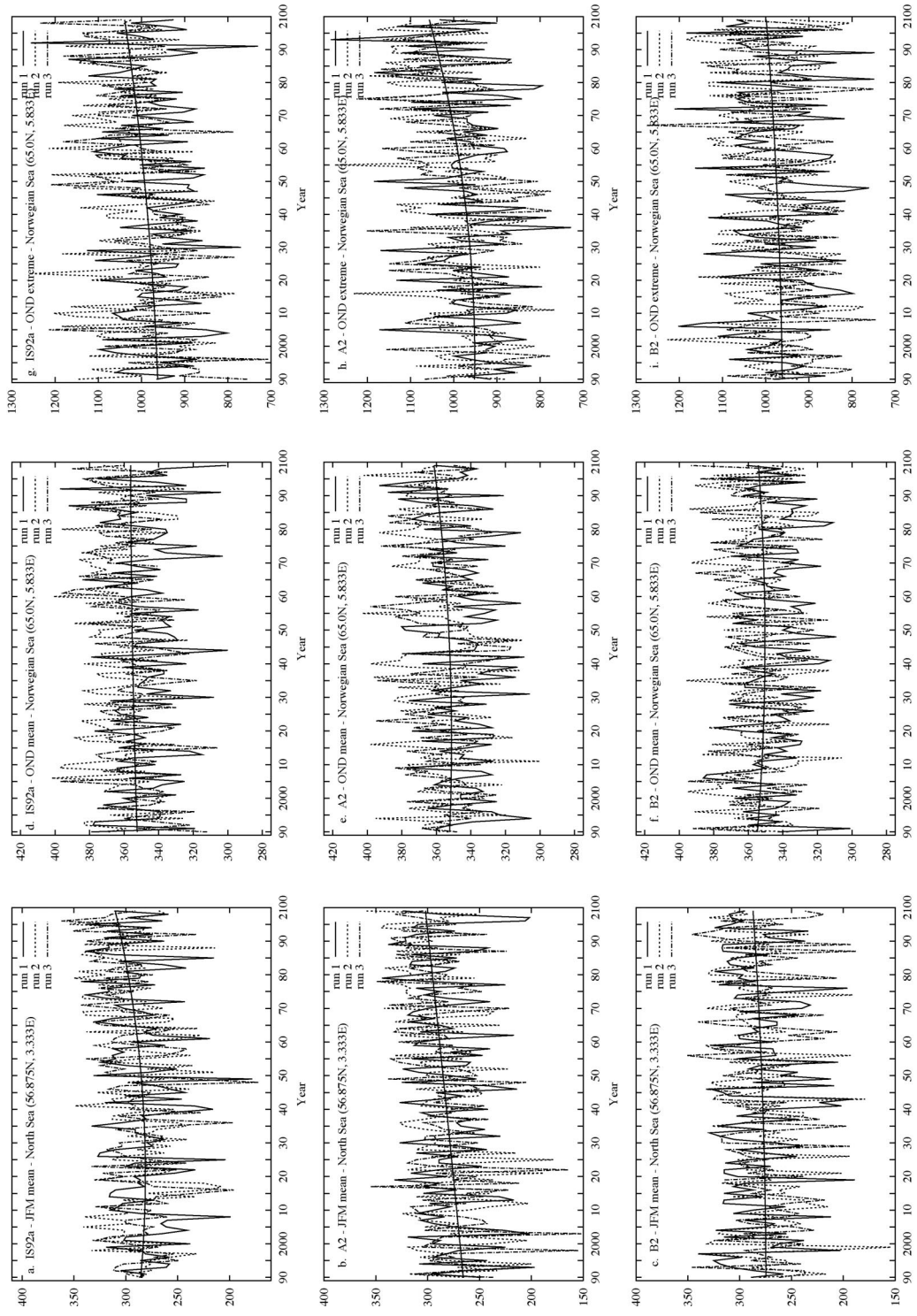

FIG. 3. Trends in winter (JFM) and fall (OND) seasonal mean (a)–(f) SWH, as well as in the location parameter μ, of the fall seasonal (g)–(i) SWH extremes, as projected with the three (IS92a, A2, and B2) forcing scenarios for the indicated grid points in the northeast Atlantic. The unit of the vertical axis is cm.

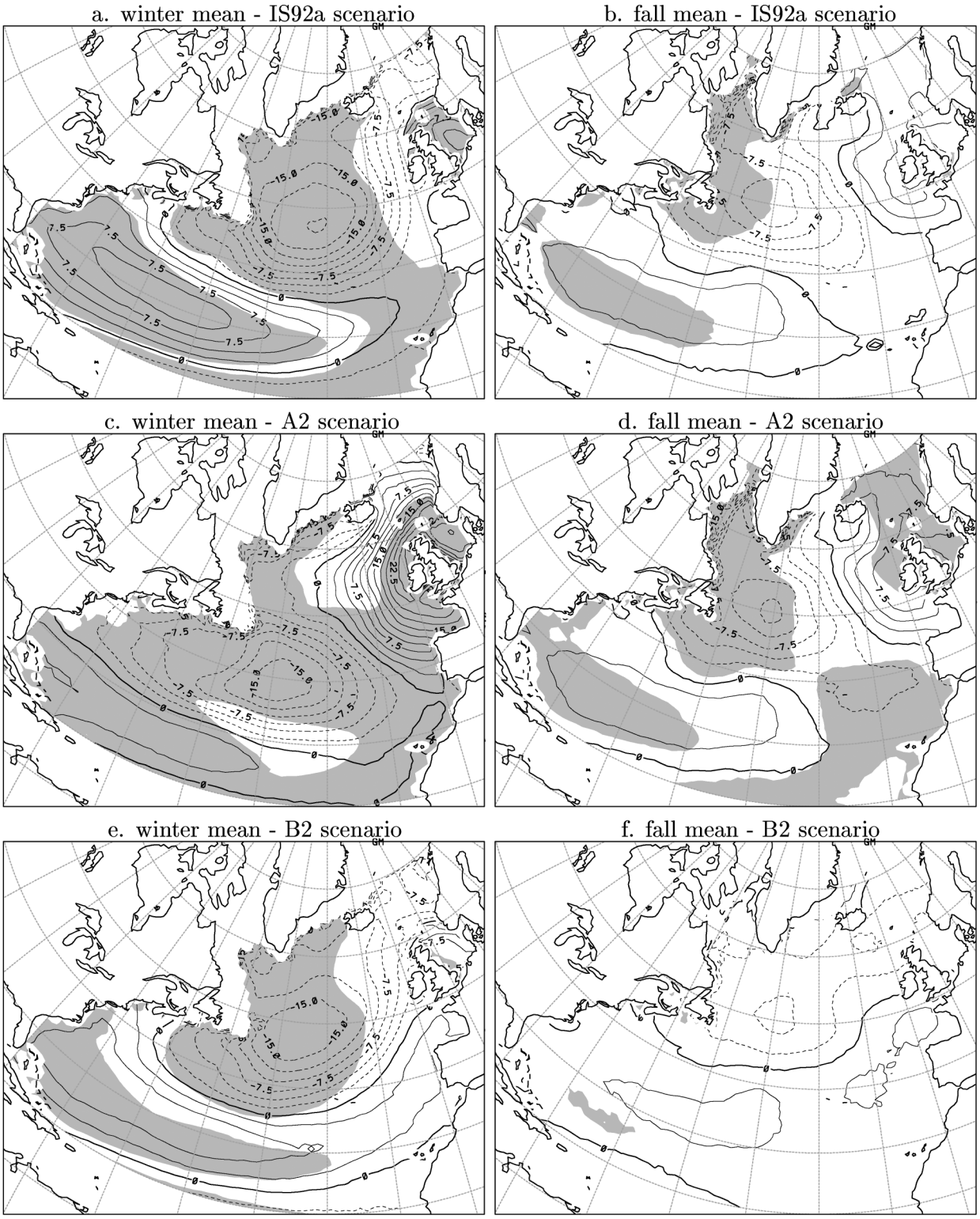

FIG. 4. Changes in the (left) winter and (right) fall seasonal means of SWH in the period from 1990 to 2080 (2080s minus 1990s), as projected with the indicated forcing scenarios. The contour interval is 2.5 cm. Solid and dashed lines are positive and negative contours, respectively. Shading indicates areas of significant quadratic trends (RM_2; see section 3b).

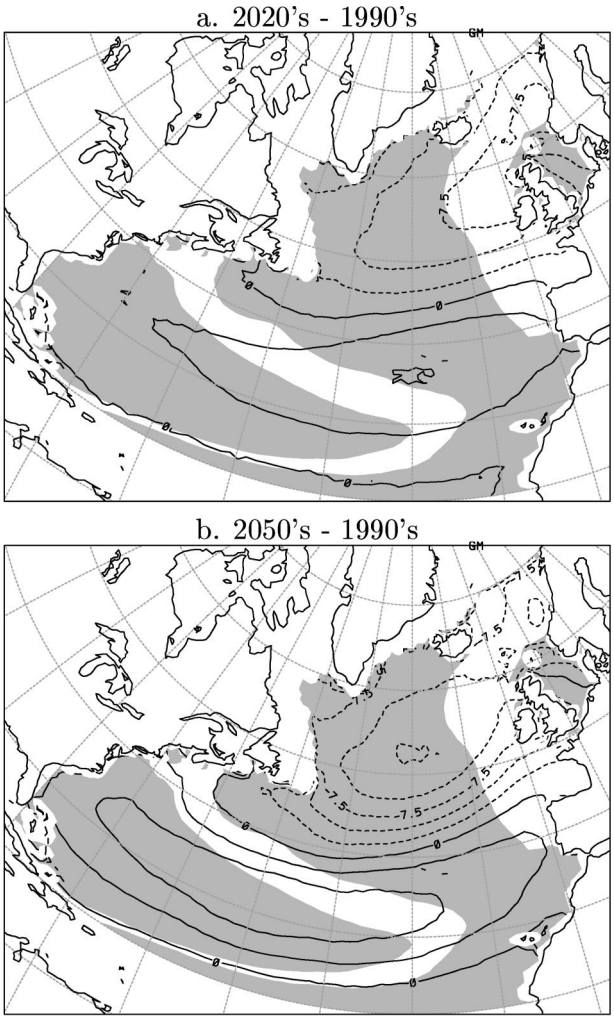

FIG. 5. The same as in Fig. 4 but for changes in the winter seasonal means of SWH from 1990 to (a) 2020 and (b) 2050, as projected with the IS92a forcing scenarios.

means of SWH in this region (cf. Fig. 4d). Again, the stronger forcing (IS92a and A2) scenarios project larger increases in fall 90th percentiles of SWH than does the weaker (B2) forcing scenario, especially in the northeast Atlantic (cf. Table 3).

b. Implications of climate change for extreme wave height events

The GEV analysis described in section 3b was carried out to explore implications of climate change for seasonal extreme wave height events. As described in section 3b, the location parameter of seasonal extreme SWH is highly correlated with both anomalies of seasonal mean SLP (P_t) and the seasonal SLP gradient index (G_t), but the scale parameter appears to be independent of both P_t and G_t. Thus we used the GEV_2 model to estimate possible future changes in the SWH extremes under the three forcing scenarios.

For each forcing scenario, a projection of the change in the location parameter of seasonal extreme SWH was obtained from each of the three ensemble members using the expression $\hat{\mu}_t = \hat{\mu}_o + \hat{r}_1 P_t + \hat{r}_2 G_t$. These three projections were analyzed in a combined trend analysis as described in section 3c. As shown in Table 3, the projected trend in the location parameter is field significant in both winter and fall. As with the SWH statistics discussed earlier, the quadratic component of trend is also significant in winter, especially for the A2 scenario.

Generally, the characteristics of quadratic trends in the location parameter of SWH extremes are similar to those in the seasonal mean SWH. In the Norwegian and North Seas, the quadratic trends again feature either faster increases in the late decades than in the first few decades (cf. Figs. 3g–i), or a decreasing trend in the first few decades followed by an increasing trend in the late decades of the 1990–2099 period (not shown, but similar to Fig. 3a). However, the projected changes in fall extreme SWH in the Norwegian Sea appear to be more nonlinear than those projected for the seasonal means under the strong forcing (IS92a and A2) scenarios (cf. Figs. 3d,e and 3g,h).

Since the quadratic components of trend in the location parameter are not negligible, the RM_2 trend model was chosen for use in estimating changes in the projected location parameter $\hat{\mu}_t$. This trend model was then substituted into the GEV_2 extreme value model described in section 3b {i.e., GEV $[\hat{\mu}_{\mathrm{tr}}(t), \hat{\sigma}, \hat{\xi}]$}, which in turn was used to estimate 20-yr return values of SWH ($H_{20\mathrm{yr}}$) for the climates of 1990, 2020, 2050, and 2080. This extreme value model was also used to estimate the return period for the 20-year circa 1990 event in the climate of the 2020s, 2050s, and 2080s. Selected results are shown in Figs. 7–9.

Increases in the extreme wave height of a fixed frequency of occurrence, or equivalently, reductions in the waiting time between extreme wave height events of a fixed size, were identified for the projected warmer climates. For example, in the Norwegian and North Seas we projected a 15–45-cm increase in the winter 20-yr return values in the 90-yr period between 1990 and 2080 (see Figs. 7a,c). Equivalently, the winter extreme wave heights that occur on average once every 20-yr period in the present-day (1990s) climate (11–13 m; see Fig. 8a) is expected to occur on average once every 12–16-yr period in the climate projected for year 2080 (cf. Fig. 9a). In fall, the situation is similar: under the strong forcing scenarios, the fall 20-yr return values of SWH in the Norwegian Sea will increase by 60–100 cm from 1990 to 2080 (cf. Fig. 7, right), or equivalently, the fall extreme wave height events that occur on average once every 20-yr period in the present-day climate is expected to occur on average once every 4–12-yr period in the climate projected for year 2080 (cf. Fig. 9b).

The patterns of changes in the 20-yr return values of SWH bear substantial similarity to the RA-projected

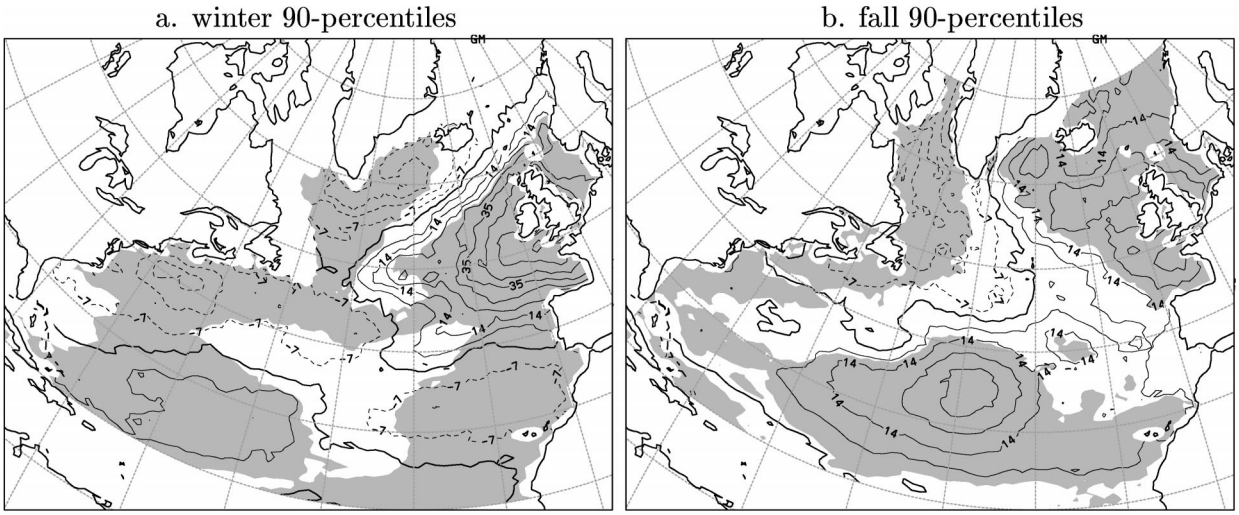

FIG. 6. The same as in Fig. 4 but for changes in the indicated seasonal 90th percentiles of SWH from 1990 to 2080, as projected with the A2 forcing scenario. The contour interval is 7 cm.

patterns of change in seasonal mean SWH (cf. Figs. 4 and 7). However, in the northeast Atlantic, increases in the seasonal extremes are much larger than those in the seasonal means in the fall season (cf. Figs. 4 and 7). The largest increases in the extreme SWH in the northeast Atlantic are now projected for the fall season rather than for the winter season.

5. Concluding remarks

While using a traditional least squares approach for downscaling climate variables that are basically Gaussian distributed, we have also demonstrated the use of a new approach for downscaling climate extremes (i.e., non-Gaussian variables). More specifically, by means of linear regression analysis and nonstationary generalized extreme analysis, we have constructed climate change scenarios for seasonal mean and extreme significant wave heights, using the CGCM2 simulations of SLP for three different forcing scenarios.

With all three forcing scenarios, the northeast Atlantic is projected to have increases in both winter and fall seasonal means and extremes of SWH in the twenty-first century. These increases are generally accompanied by decreases in the midlatitudes of North Atlantic and increases in the southwest North Atlantic.

The GEV analysis shows that global warming may result in changes in the location parameter of the distribution of wave height extremes, eventually leading to changes in the size and frequency of extreme wave height events. For example, in the Norwegian Sea, an extreme wave height event that occurs on average once every 20-yr period in fall in the present-day (1990s) climate is expected to occur on average once every 4–12 yr in the climate projected for year 2080 under the A2 forcing scenario. Such significant changes will have an impact on the life span of marine and coastal infrastructure in the area. The possible changes in future wave extremes should be taken into account in the design, planning, and operation of coastal and offshore industries.

The changes in significant wave heights projected for the 1990–2099 period are not simply linear. In the Norwegian and North Seas, the nonlinearity is characterized either by faster increases in the late decades than in the first few decades, or by decreases in the first few decades followed by increases. Also, it was shown that similar forcing scenarios lead to similar changes in ocean waves, and that a scenario with a slower rate of increase in GHG forcing leads to a slower rate of change in ocean waves.

The projected changes in the wave height climate are consistent with the corresponding climate changes that are projected to occur in SLP. As shown in Fig. 10 (A2 scenario), global warming leads to decreases in SLP over the northeast Atlantic, accompanied with increases over the midlatitudes (cf. red contours in Fig. 10), which results in an increased pressure gradient over the northeast Atlantic. This change in pressure gradient results in stronger westerly winds and more frequent occurrence of strong cyclones (central pressure lower than 990 mb) that affect the northeast Atlantic and northern European coasts (Wang et al. 2004, manuscript submitted to *J. Climate*), and hence increases of SWH in the northeast Atlantic. For example, the 1010-mb contour shifts from over Norway to over Denmark (see the dark green shading edge and the thick black contour line in Fig. 10), resulting in an increased pressure gradient and stronger westerly winds over the region.

It is possible that anthropogenic forcing may affect the ocean wave climate by changing the occupation statistics of atmospheric circulation regimes. Using the CGCM1 simulations of the Canadian Centre for Climate Modelling and Analysis, Monahan et al. (2000) con-

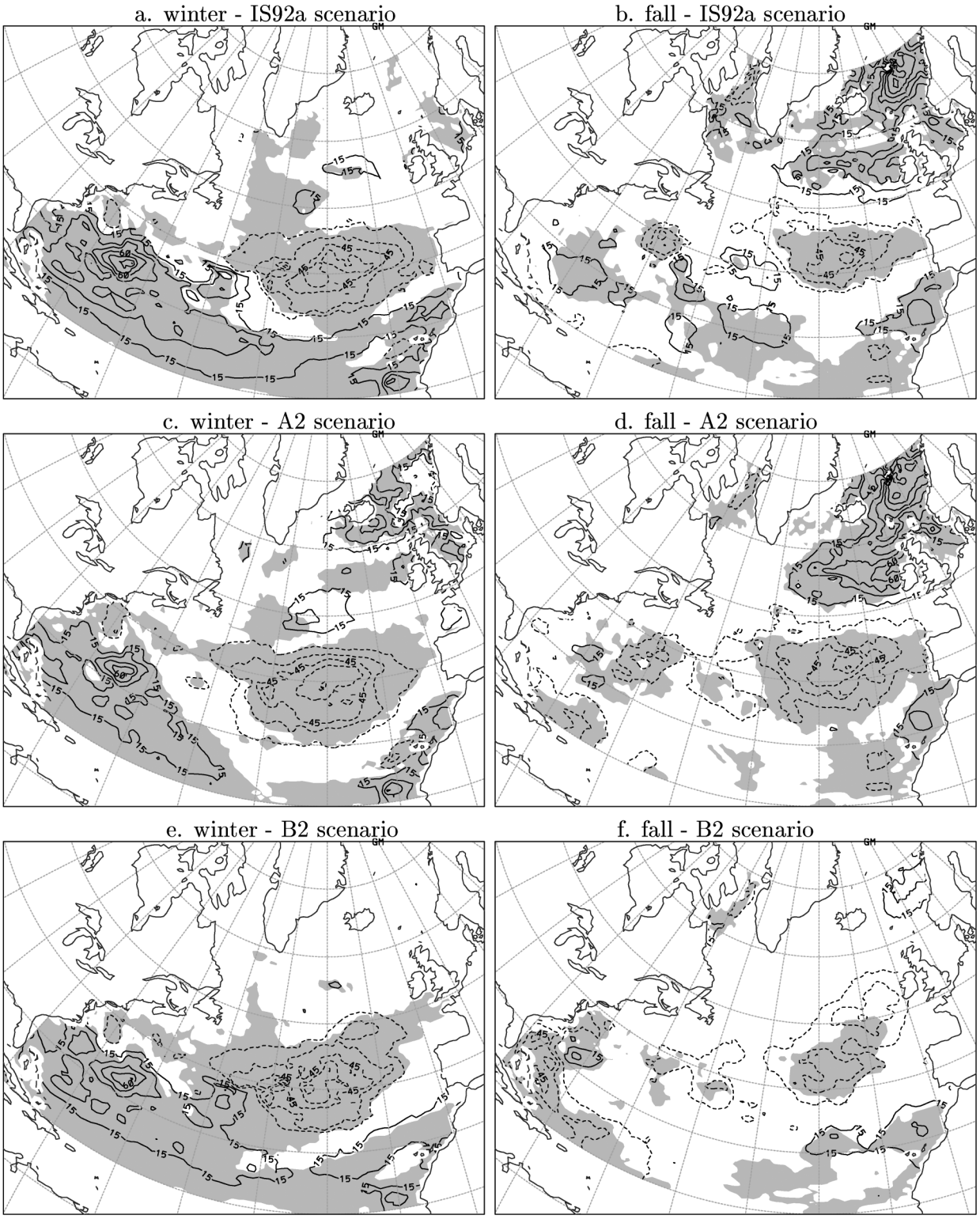

FIG. 7. Changes in the (left) winter and (right) fall 20-yr return values of SWH (H_{20yr}) from 1990 to 2080 (2080s minus 1990s), as projected with the indicated forcing scenarios. The contour interval is 15 cm. Solid and dashed lines indicate positive and negative contours, respectively. Shading indicates areas of significant quadratic trends in the location parameter of the SWH extremes.

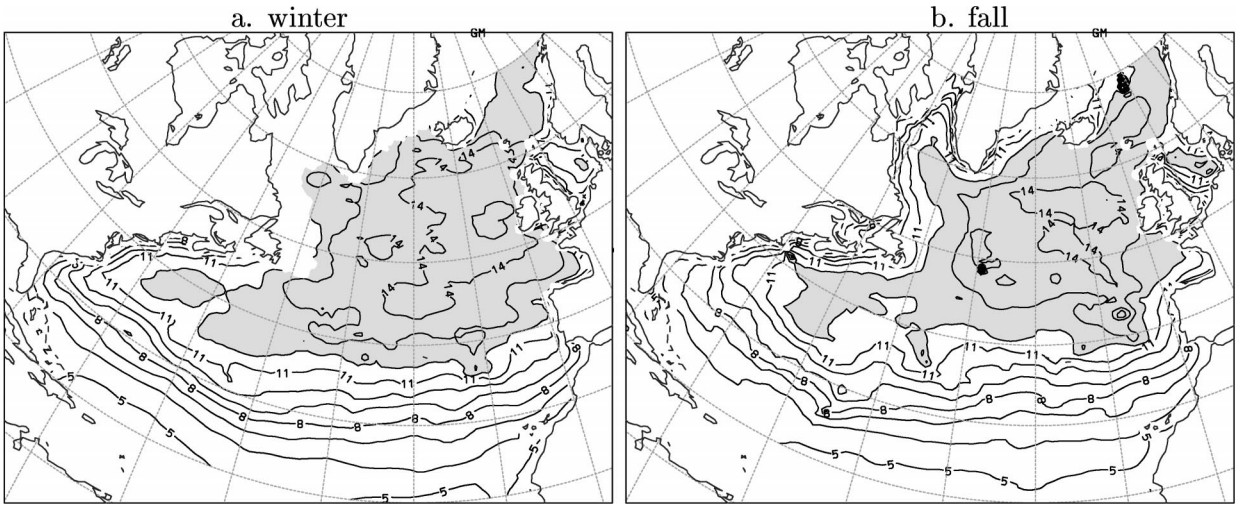

FIG. 8. The 20-yr return values of SWH (H_{20yr}), estimated using the GEV parameters of year 1990 for the indicated seasons (A2 scenario). The contour interval is 1.0 m. Shading indicates areas of values ≥12 m.

cluded that under global warming, the episodic split-flow regime [which resembles the extreme negative phase of the North Atlantic Oscillation (NAO) in SLP] occurs less frequently while the standing oscillation regime (which resembles the Arctic Oscillation) occurs more frequently. In other words, global warming is associated with more frequent occurrence of the positive phase of NAO on the one hand, and with increases of wave height in the northeast Atlantic on the other hand. The implication here is that the projected wave height increases in the northeast Atlantic are associated with the anthropogenic changes that affect the NAO. Such a relationship between the NAO and wave height makes sense physically and is well supported by observational evidence. The significant increases in winter wave height observed in the northeast Atlantic in 1958–97 were found to be closely related to an ''enhanced'' positive phase of NAO (Wang and Swail 2001, 2002).

For the northeast Atlantic, our scenarios are consistent with the double CO_2 scenario of the STOWASUS-2100 (Kaas and the STOWASUS Group 2001), in which the mean SWH in this region was projected to have 5–35-cm increases in the climate of 2060–89 relative to that of 1970–99 in the cold seasons (September–February; Kaas and the STOWASUS Group (2001; 128–129). Correspondingly, our scenarios projected 5–35-cm (5–20 cm) increases in the climate of 2070–99 relative to the 1961–90 climate for winter (fall) mean SWH (not shown).

Note that the basic assumption in this study is that

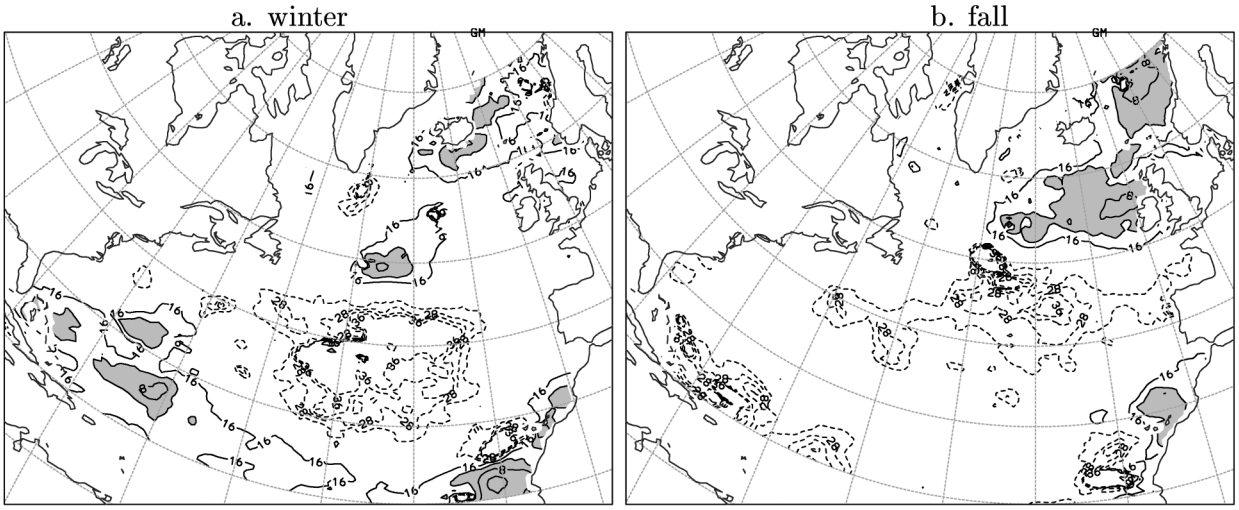

FIG. 9. Future return periods of the 1990s H_{20yr}, as estimated using the GEV parameters values projected for year 2080 using the A2 forcing scenario. The contour interval is 4 yr. Solid and dashed contours indicate return periods shorter and longer than 20 yr, respectively (20-yr contours not drawn). Shading indicates areas of values ≤12 yr.

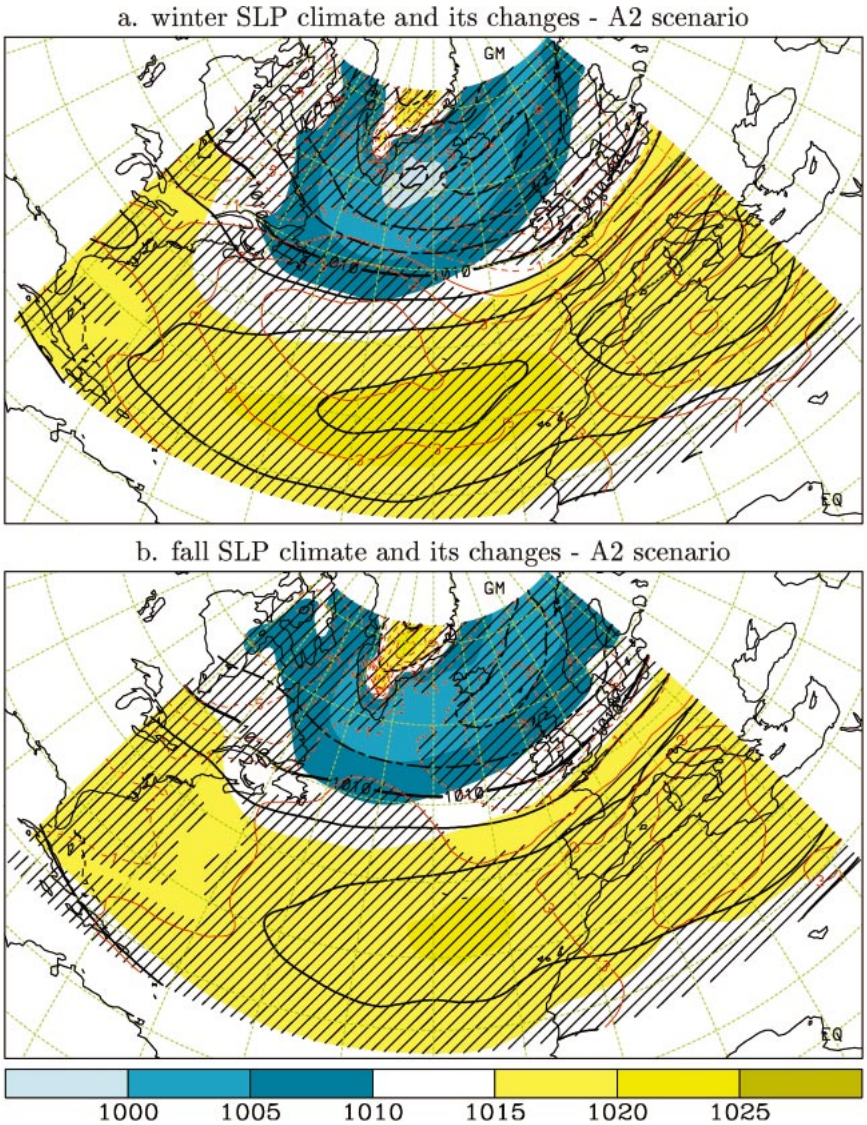

FIG. 10. The climate (30-yr mean) field of (a) winter and (b) fall SLP for 1961–90 (1970s; shaded contour map) and of 2070–99 (2080s; thick black line contour map; contour interval 5 hPa). The red contours show the difference between the two climates [2080s − 1970s; contour interval is 1 hPa; dashed (solid) red lines indicate decreases (increases); zero contours are in bold]; hatching indicates areas of significant (at 5% level) climate change.

the SLP–SWH relationship developed for the present-day climate will continue to hold under the different forcing conditions of possible future climates. Although the empirical-based technique is economical and practical, it cannot account for possible systematic changes in regional forcing conditions or feedback processes. The various sources of uncertainty related to climate scenario construction should be kept in mind when interpreting/using the climate change scenarios. However, we reiterate that the SLP–SWH relationships that we diagnosed from observations should be reasonably robust. Those relationships rely primarily on the large-scale structure of the North Atlantic SLP field as represented by its low-order EOFs. These EOFs represent the model-simulated SLP variability well, both in the twentieth century and in climates projected for the twenty-first century. Thus the modes of SLP variability that are linked to SWH variability in the present-day climate should continue to be influential in determining SWH variability in the future climate.

Acknowledgments. The GEV analysis described in this paper was performed in the statistical language S-PLUS, using functions developed by the authors in combination with functions downloaded from the URL http://www.maths.bris.ac.uk/masgc/ismev/summary.html (see appendix A in Coles 2001). We very much appre-

ciate the fact that S. Coles has made these tools freely available to the scientific community.

REFERENCES

Boer, G. J., G. Flato, M. C. Reader, and D. Ramsden, 2000: A transient climate change simulation with greenhouse gas and aerosol forcing: Experimental design and comparison with the instrumental record for the twentieth century. *Climate Dyn.,* **16,** 405–425.

Chang, E. K. M., and Y. Fu, 2003: Using mean flow change as a proxy to infer interdecadal storm track variability. *J. Climate,* **16,** 2178–2196.

Coles, S., 2001: *An Introduction to Statistical Modeling of Extreme Values.* Springer-Verlag, 208 pp.

Cox, A. T., V. J. Cardone and V. R. Swail, 2001: On the use of in situ and satellite wave measurements for evaluation of wave hindcasts. *Guide to the Applications of Marine Climatology, Part II,* World Meteorological Organization, in press.

Flato, G. M., and G. J. Boer, 2001: Warming asymmetry in climate change simulations. *Geophys. Res. Lett.,* **28,** 195–198.

Gillett, N. P., F. W. Zwiers, A. J. Weaver, and P. A. Stott, 2003: Detection of human influence on sea level pressure. *Nature,* **422,** 292–294.

Houghton, J. T., Y. Ding, D. J. Griggs, M. Noguer, P. J. van der Linden, X. Dai, K. Maskell, and C. A. Johnson, Eds., 2001: *Climate Change 2001: The Scientific Basis.* Cambridge University Press, 881 pp.

Kaas, E., and the STOWASUS Group, cited 2001: Regional storm, wave and surge scenarios for the 2100 century (STOWASUS-2100). Final report. [Available online at http://www.dmi.dk/pub/STOWASUS-2100/.]

Kalnay, E., and Coauthors, 1996: The NCEP/NCAR 40-Year Reanalysis Project. *Bull. Amer. Meteor. Soc.,* **77,** 437–471.

Lau, N.-C., 1988: Variability of the observed midlatitude storm tracks in relation to low-frequency changes in the circulation pattern. *J. Atmos. Sci.,* **45,** 2718–2743.

Leadbetter, M. R., G. Lindgren, and H. Rootzen, 1983: *Extremes and Related Properties of Random Sequences and Processes.* Spring Verlag, 336 pp.

Livezey, R. E., and W. Y. Chen, 1983: Statistical field significance and its determination by Monte Carlo techniques. *Mon. Wea. Rev.,* **111,** 46–59.

Monahan, A. H., J. C. Fyfe, and G. M. Flato, 2000: A regime view of Northern Hemisphere atmospheric variability and change under global warming. *Geophys. Res. Lett.,* **27,** 1139–1142.

Nakicenovic, N., and R. Swart, Eds., 2000: *Special Report on Emissions Scenarios (SRES).* Cambridge University Press, 570 pp.

Palmer, T. N., 1999: A nonlinear dynamical perspective on climate prediction. *J. Climate,* **12,** 575–591.

Swail, V. R., and A. T. Cox, 2000: On the use of NCEP–NCAR reanalysis surface marine wind fields for a long-term North Atlantic wave hindcast. *J. Atmos. Oceanic Technol.,* **17,** 532–545.

Tyler, D. E., 1982: On the optimality of the simultaneous redundancy transformations. *Psychometrika,* **47,** 77–86.

Venables, W. N., and B. D. Riplay, 1999: *Modern Applied Statistics with S-PLUS.* 3d ed. Springer, 501 pp.

von Storch, H., and F. W. Zwiers, 1999: *Statistical Analysis in Climate Research.* Cambridge University Press, 484 pp.

Wang, X. L., and V. R. Swail, 2001: Changes of extreme wave heights in Northern Hemisphere oceans and related atmospheric circulation regimes. *J. Climate,* **14,** 2204–2221.

——, and F. W. Zwiers, 2001: Using redundancy analysis to improve dynamical seasonal mean 500 hPa geopotential forecasts. *Int. J. Climatol.,* **21,** 637–654.

——, and V. R. Swail, 2002: Trends of Atlantic wave extremes as simulated in a 40-yr wave hindcast using kinematically reanalyzed wind fields. *J. Climate,* **15,** 1020–1035.

WASA Group, 1998: Changing waves and storms in the Northeast Atlantic? *Bull. Amer. Meteor. Soc.,* **79,** 741–760.